Nano Energy 136 (2025) 110690

Contents lists available at ScienceDirect

Nano Energy

journal homepage: www.elsevier.com/locate/nanoen

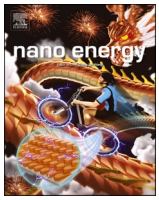

Lead-free GeTe alloys with high thermoelectric performance for low-grade waste heat energy harvesting

Haiqi Li [a], Chen Chen [b,*], Jinxuan Cheng [c], Yuanhang Xia [a], Shuang Lyu [a], Kejia Liu [a], Wenhua Xue [c], Dongyi Shen [a], Wenxuan Wang [a], Qian Zhang [c,*], Yue Chen [a,*]

[a] Department of Mechanical Engineering, The University of Hong Kong, Pokfulam Road, Hong Kong SAR, PR China
[b] Dongguan Key Laboratory of Interdisciplinary Science for Advanced Materials and Large-Scale Scientific Facilities, School of Physical Sciences, Great Bay University, Dongguan, Guangdong 523000, PR China
[c] School of Materials Science and Engineering, Harbin Institute of Technology, Shenzhen 518055, PR China

ARTICLE INFO

Keywords:
Thermoelectrics
GeTe
Lead-free
Band convergence
Conversion efficiency

ABSTRACT

Harvesting and utilization of low-grade waste heat dissipated from industries have garnered immense attention in recent years. Thermoelectric materials, which can directly convert heat into electricity, provide an eco-friendly solution for waste heat recovery. Recently, GeTe-based materials have developed as strong competitors to Bi_2Te_3 near room temperature. Nonetheless, despite exhibiting comparable thermoelectric performance, the majority of these GeTe alloys incorporate toxic Pb, thus limiting the practical application. Herein, a boosted zT was achieved in $Ge_{0.93}Bi_{0.05}Te$ over the entire temperature range by introducing Ge deficiency. Further $AgSbTe_2$ alloying leads to a remarkable increase in density-of-states effective mass and high weighted mobility. Thermally, the addition of $AgSbTe_2$ forms various phonon scattering centers including domain structures, dislocations, and phase boundaries, contributing to the low lattice thermal conductivity. As a result, a high average zT of 1.34 (323–573 K) is obtained in the lead-free $(Ge_{0.93}Bi_{0.05}Te)_{85}(AgSbTe_2)_{15}$ material, and its maximum single-leg conversion efficiency reaches 8.6 % at $\Delta T = 273$ K. The outstanding thermoelectric performance and the lead-free characteristic presented in our study shed light on the potential of GeTe alloys for applications in recovering low-grade waste heat.

1. Introduction

The low-grade waste heat (below 600 K) occupies the largest proportion (over 50 %) of industrial combustion emissions. [1] For reusing this abundant low-grade heat, thermoelectric materials that can achieve direct heat-to-electricity conversion, has garnered immense research interest. The energy conversion efficiency, which is primarily dominated by the material's dimensionless figure-of-merit zT, defined by $zT = \sigma S^2 T/(\kappa_e + \kappa_L)$, where σ, S, T, κ_e, and κ_L represent the electrical conductivity, the Seebeck coefficient, the absolute temperature, the electronic, and lattice thermal conductivity, respectively. Bi_2Te_3-based compounds have long been recognized as ideal thermoelectric materials for low-grade heat recovery owing to their high zT values at around room temperature. However, they experience a dramatic decrease in zT values above ~400 K due to the bipolar effect, [2] leading to the deterioration of thermoelectric performance. Over the past few years, significant efforts have been dedicated to developing non-Bi_2Te_3 thermoelectric materials for recovering the low-grade waste heat, including compounds based on MgAgSb, [3] Mg_3Sb_2, [4] PbSe, [5] $AgSbTe_2$, [6] and SnSe. [7]

GeTe, a thermoelectric material within IV-VI group, has been extensively studied and demonstrated exceptional thermoelectric performance (peak $zT > 2$) in the mid-temperature range (600–900 K). Recently, researchers have developed various approaches to enhance the zT value of p-type GeTe-based materials in the low-temperature range, making them competitors to Bi_2Te_3-based alloys. These strategies include bandgap manipulation, [8] increasing the density of states (DOS) near the Fermi level by converging multiple energy bands [9–11] or introducing resonant states [12,13] to enhance the electrical transport performance. On the thermal side, the reduction of lattice thermal conductivity can be achieved by introducing interstitial atoms, [14] point defects, [15,16] stacking faults, [17] dislocations [18], and nano inclusions. [19] Bu *et al.* obtained a high band degeneracy (N_v), leading to a zT of 1.1 at 350 K in $Ge_{0.42}Pb_{0.58}Te$. [20] Jiang *et al.* optimized the

* Corresponding authors.
E-mail addresses: ccmldn@gbu.edu.cn (C. Chen), zhangqf@hit.edu.cn (Q. Zhang), yuechen@hku.hk (Y. Chen).

https://doi.org/10.1016/j.nanoen.2025.110690
Received 1 August 2024; Received in revised form 19 December 2024; Accepted 18 January 2025
Available online 20 January 2025

electron and phonon localization through high entropy engineering, achieving a zT of 0.6 at room temperature in $Ge_{0.61}Ag_{0.11}Sb_{0.13}Pb_{0.12}Bi_{0.01}Te$, along with a conversion efficiency of 7.6 % using a segmented module under a temperature difference of 260 K. [21] Qiu *et al.* obtained a zT of 0.5 at 300 K and an average zT of 1.06 from 300 K to 573 K in $Ge_{0.84}In_{0.01}Pb_{0.1}Sb_{0.05}Te_{0.997}I_{0.003}$ by cooperatively optimizing electrical and thermal properties. [22] Nonetheless, the majority of the above-mentioned approaches in GeTe-based compounds involve toxic Pb alloying, limiting practical production. Therefore, developing Pb-free GeTe alloys with high thermoelectric performance is the main striving direction for future research.

In this work, we successfully achieved a synergetic optimization of electrical and thermal transport properties by the introduction of Ge deficiency and $AgSbTe_2$ alloying, obtaining an excellent weighted mobility μ_w and a lower lattice thermal conductivity κ_l among other reported lead-free GeTe compounds, [23–34] as shown in Fig. 1a. For the electrical transport properties, the addition of Ge deficiency and high-symmetry $AgSbTe_2$ facilitates the phase transition from rhombohedral GeTe to cubic GeTe, leading to an increase in the density-of-states effective mass m^*, which ultimately improves the electrical transport performance. Regarding the thermal transport properties, the formation of multiscale hierarchical defects including domain structures, dislocations, phase boundaries, and point defects, efficiently scatter a wide range of phonons, resulting in ultra-low lattice thermal conductivity. As a consequence, a high zT of 0.73 at 323 K and a high average zT of 1.34 over 323–573 K were obtained in $(Ge_{0.93}Bi_{0.05}Te)_{85}(AgSbTe_2)_{15}$ among lead-free GeTe-based compounds, [23,34–38] as shown in Figs. 1b and 1c. For the prepared single leg, a conversion efficiency (η) of 8.6 % was achieved when the temperature difference (ΔT) was 273 K. Such a high η overperforms most reported Bi_2Te_3-based, [39–45] TAGS-based, [46,47] and lead-free GeTe-based [34,37,48] modules (Fig. 1d). This work provides a perspective on the advancement of GeTe-based modules as the next-generation low-temperature thermoelectric power generators.

2. Results and discussion

2.1. Effects of Ge deficiency on optimizing the TE properties of $Ge_{0.95-x}Bi_{0.05}Te$

The room-temperature X-ray diffraction (XRD) patterns of $Ge_{0.95-x}Bi_{0.05}Te$ ($x = 0$, 0.02, and 0.04) match the rhombohedral structure (PDF#47–1079, *Rm* space group), as shown in Fig. S1, and the Ge precipitates disappear upon the introduction of Ge deficiency. Fig. 2a-c displays the electrical conductivity, Seebeck coefficient, and power factor of $Ge_{0.95-x}Bi_{0.05}Te$ samples. In Fig. 2a, the electrical conductivity is almost constant when $x = 0$ and 0.02; however, an obvious increase is observed when x reaches 0.04. This increase can be ascribed to the heightened carrier concentration resulting from the increased cation vacancies (Ge^{2+}), as shown in Fig. S2. As expected, the Seebeck coefficient exhibits the opposite tendency due to its coupled relationship with electrical conductivity (Fig. 2b). To further explore the impact of Ge deficiency in the band structure, the Pisarenko plot is drawn in Fig. 2d,

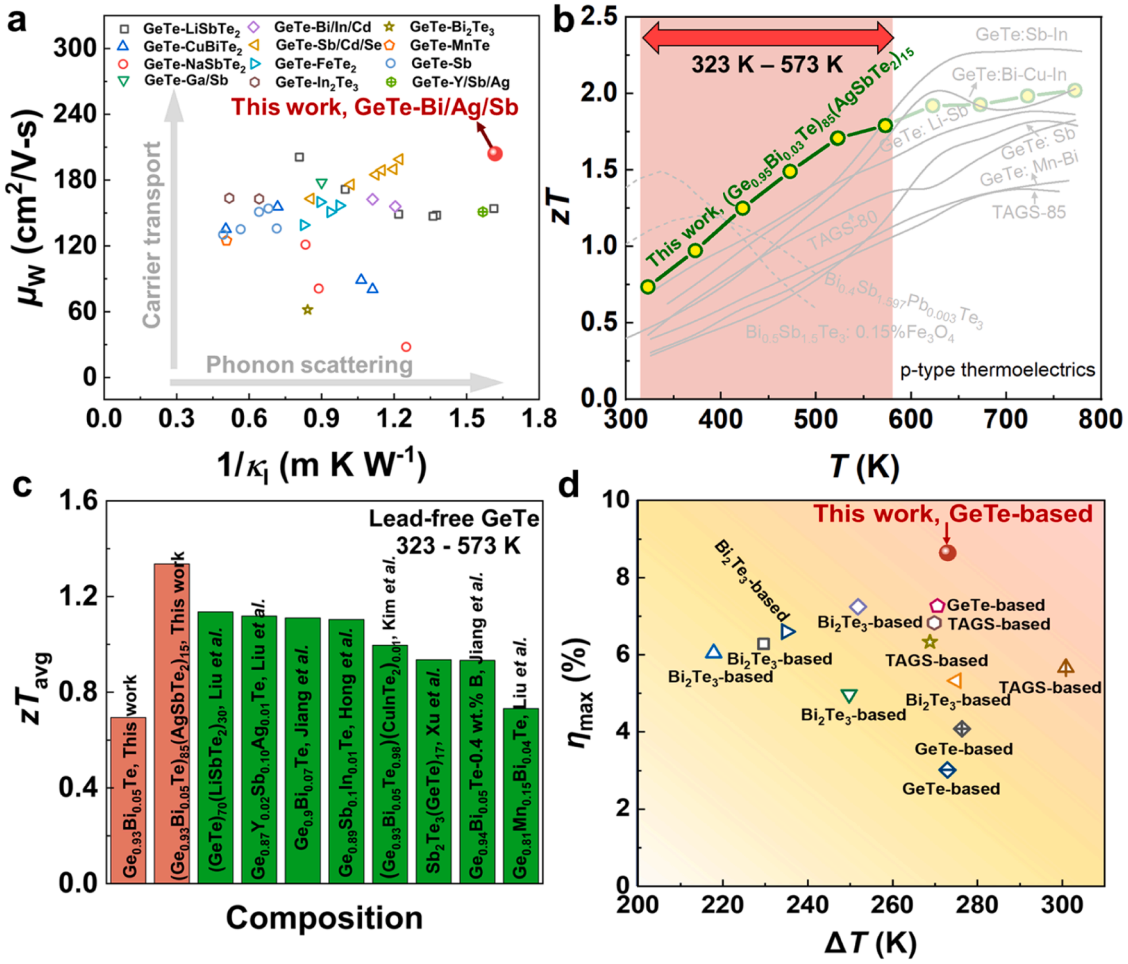

Fig. 1. Thermoelectric performance of $(Ge_{0.93}Bi_{0.05}Te)_{85}(AgSbTe_2)_{15}$ compared with other reported Bi_2Te_3-based, [39–45,49,50] TAGS-based, [46,47,51,52] and lead-free GeTe-based [23,34–38,48,53] data; a, The μ_w versus $1/\kappa_l$ at 323 K. **b,** Temperature-dependent zT value. **c,** Average zT from 323 K to 573 K. **d,** The maximum thermoelectric conversion efficiency.

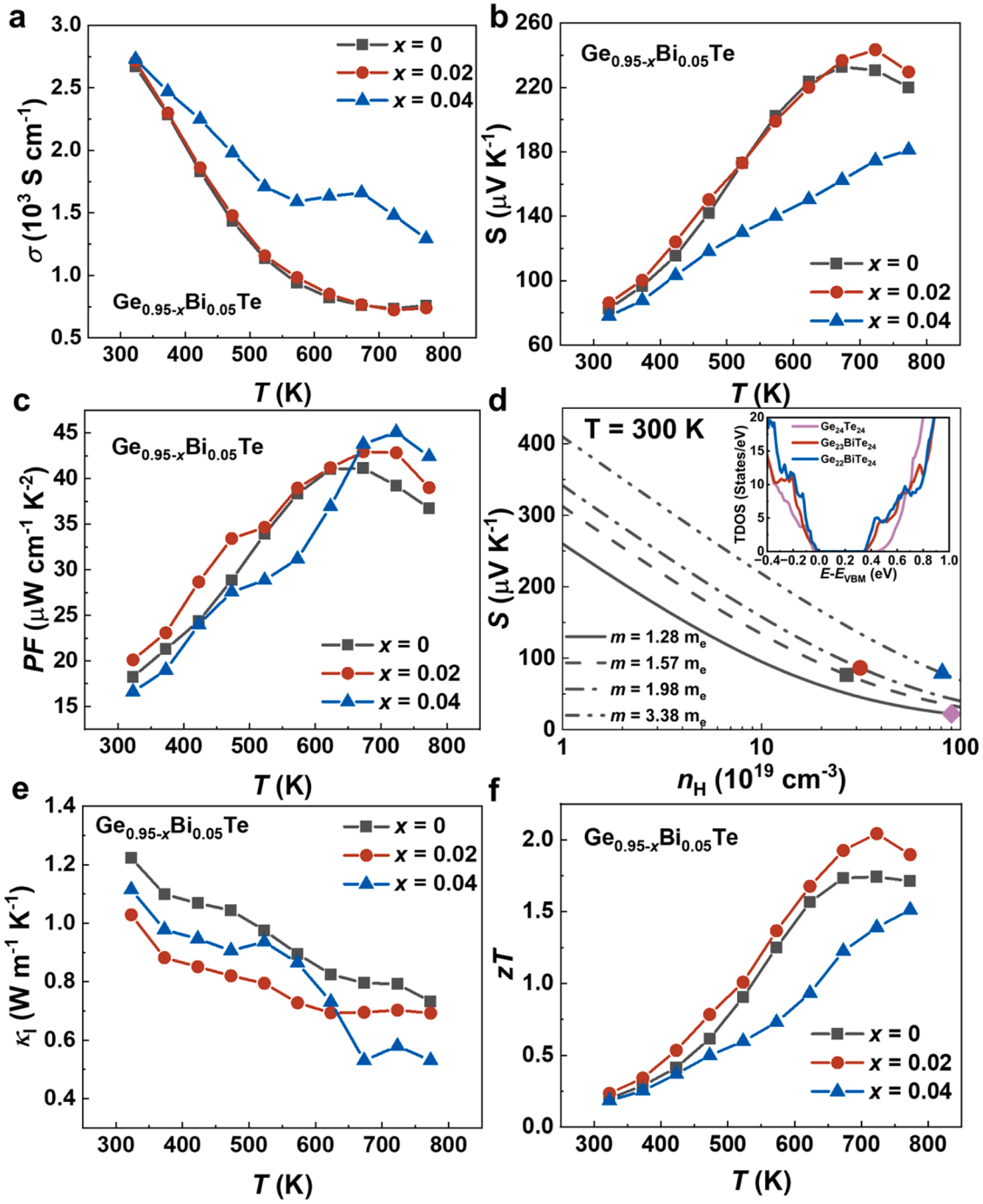

Fig. 2. Thermoelectric properties and Pisarenko relations for $Ge_{0.95-x}Bi_{0.05}Te$ ($x = 0$, 0.02, and 0.04). Temperature-dependent thermoelectric properties: **a,** Electrical conductivity; **b,** Seebeck coefficient; **c,** Power factor; **e,** Lattice thermal conductivity; **f,** zT values. Carrier concentration-dependent Seebeck coefficient at 300 K compared to the reported value for pristine GeTe (purple diamond), [55] and density-of-states (the inset) of $Ge_{24}Te_{24}$, $Ge_{23}BiTe_{24}$, and $Ge_{22}BiTe_{24}$ are given in panel **d**.

considering the single parabolic band (SPB) model. [54] The density-of-states effective mass (m^*) continuously increases from 1.57 m_e to 3.38 m_e upon the introduction of Ge deficiency, where m_e is the electron mass. We also performed DFT calculations to elucidate the increase in effective mass, as depicted in the inset of Fig. 2d, where the valence band maximum (VBM) has been shifted to 0 eV. A rise in the DOS of the top of the valence band can be observed with decreasing Ge concentration, suggesting that the introduction of Ge deficiency can modulate the band structure and enhance the effective mass of $Ge_{0.95}Bi_{0.05}Te$.

The total thermal conductivity (κ) of $Ge_{0.95-x}Bi_{0.05}Te$ ($x = 0$, 0.02, and 0.04) is displayed in Fig. S3a. The lattice thermal conductivity (κ_l), as presented in Fig. 2e, is obtained by subtracting κ_e from κ ($\kappa_l = \kappa - \kappa_e$), where κ_e represents the temperature-dependent electronic thermal conductivity, calculable using the Wiedemann-Franz law.

Notably, the $x = 0.02$ sample exhibits lower lattice thermal conductivity compared to other samples. A similar phenomenon was also observed by Tsai *et al.*, [56] though the underlying reasons for this behavior may be more complex. The κ experiences an increase when $x = 0.04$, primarily arising from the increased electronic thermal

conductivity (Fig. S3b) caused by the higher carrier concentration. Benefiting from the boosted effective mass and reduced lattice thermal conductivity, $Ge_{0.93}Bi_{0.05}Te$ achieves the best thermoelectric performance among all samples across the entire temperature range, and the peak zT reaches about 2.04 at 723 K (Fig. 2 f).

2.2. Synergistic optimization of electrical and thermal performances by alloying with $AgSbTe_2$

Although introducing Ge deficiency successfully enhances the effective mass, the Seebeck coefficient is still at a relatively low level. Previous reports have indicated that a slight symmetry reduction of cubic GeTe can effectively enhanced the density-of-states effective mass m^*, [57] which results in a higher Seebeck coefficient. Therefore, the high-symmetry cubic $AgSbTe_2$ is selected to alloy with $Ge_{0.93}Bi_{0.05}Te$ for further boosting the thermoelectric performance.

The room-temperature XRD patterns for $(Ge_{0.93}Bi_{0.05}Te)_{100-y}(AgSbTe_2)_y$ ($y = 0$, 10, 13, 15, and 17) are illustrated in Fig. 3a. All the peaks can be indexed to the low-temperature rhombohedral structure (PDF#47–1079, *Rm* space group). With the increase of $AgSbTe_2$ content, the double peaks in the 2θ range of 41–44° move closer, indicating a gradual transition from the rhombohedral phase to the cubic phase. In Fig. 3b, the temperature-dependent X-ray diffraction depicts the rhombohedral-cubic transition temperature falls within the range of 473 K to 523 K for $(Ge_{0.93}Bi_{0.05}Te)_{85}(AgSbTe_2)_{15}$, compared to ~700 K for the pristine GeTe, [58] which further confirms that $AgSbTe_2$ alloying can effectively promote the transition to the cubic structure.

The temperature-dependent thermoelectric properties of $(Ge_{0.93}Bi_{0.05}Te)_{100-y}(AgSbTe_2)_y$ ($y = 0$, 10, 13, 15, and 17) are displayed in Fig. 4. The electrical conductivity exhibits a decrease as temperature increases, indicating a heavily doped semiconductor behavior. In Fig. 4a, with the increasing $AgSbTe_2$ content, the electrical conductivity decreases, except for $y = 17$. This exception can be attributed to an obvious increase in n_H and nearly constant μ_H compared to $y = 15$, as displayed in Fig. S4. Moreover, it is counter-intuitive that the Seebeck coefficient increases as the carrier concentration rises (Fig. S4), increasing from ~86 $\mu V\ K^{-1}$ for $y = 0$ to ~169 $\mu V\ K^{-1}$ for $y = 15$ at 323 K (Fig. 4b). To better understand the enhanced Seebeck coefficient, Pisarenko relations are drawn in Fig. 4c based on the single parabolic band (SPB) model, and they are presented alongside literature results for comparison. The density-of-states effective mass (m^*) experiences a dramatic increase from 1.98 m_e for $Ge_{0.93}Bi_{0.05}Te$ to ~10.0 m_e for the alloyed samples of $(Ge_{0.93}Bi_{0.05}Te)_{100-y}(AgSbTe_2)_y$ ($y = 13$, 15 and 17), which is much higher than other GeTe alloys. [18,59–61] To further investigate the increased m^*, the electronic band structures of $Ge_{22}BiTe_{24}$ and $Ge_{16}BiAg_3Sb_3Te_{24}$ were calculated, as illustrated in Fig. S5. The incorporation of $AgSbTe_2$ reduces the energy differences between the valence band edges and significantly increases the DOS near the VBM (Fig. S6), resulting in the observed enhancement of m^*. As discussed above, the reduction in electrical conductivity can be ascribed to strong carrier-carrier scattering and the boosted effective mass.

To better estimate the carrier transport properties in relation to electronic band structure, we introduce the weighted mobility μ_w, defined as: $\mu_w = \mu_H (m^*/m_e)^{3/2}$, [62] where μ_H denotes the Hall mobility. Despite $AgSbTe_2$ alloying decreases the carrier mobility, the weighted mobility still maintains a relatively high value of ~180 $cm^2\ V^{-1}\ s^{-1}$ for $y = 13$, 15, and 17 (Fig. S7), which can be ascribed to the remarkable enhancement in the density-of-states effective mass (m^*), as shown in Table S1. Benefiting from the enhanced weighted mobility, a high average power factor of ~31 $\mu Wcm^{-1}K^{-2}$ is attained in $(Ge_{0.93}Bi_{0.05}Te)_{85}(AgSbTe_2)_{15}$ within the low-temperature range of 323 K to 573 K (Fig. 4d).

In terms of thermal transport properties, as displayed in Fig. 4e, the total thermal conductivity (κ) significantly declines with increasing $AgSbTe_2$ content across the entire temperature range, except $y = 17$. This alteration arises from the rise in electronic thermal conductivity caused by the heightened electrical conductivity (Fig. 4a). Moreover, the lattice thermal conductivity (κ_l) of the alloys reduces with the rising fraction of $AgSbTe_2$ alloying, and it reaches a minimum of about 0.62 $W\ m^{-1}K^{-1}$ at 323 K when $y = 15$. Across the entire temperature span, the lowest κ_l (~0.5 $W\ m^{-1}K^{-1}$) is achieved in $(Ge_{0.93}Bi_{0.05}Te)_{83}(AgSbTe_2)_{17}$ at 623 K, which is comparable to the theoretical minimum κ_l of GeTe estimated using the Cahill model. [64] The reduction in the lattice thermal conductivity can be partially ascribed to strong point defects scattering due to the high alloying concentration. To quantitatively explore the impact of point defects on phonon scattering, the Debye-Callaway model is introduced to predict the relaxation time of point defect scattering τ_{PD}^{-1} at room temperature. More details about this model can be found in the Supplementary Materials. The addition of $AgSbTe_2$ induces an augmentation in both mass and strain field fluctuations (Fig. S8), leading to a shorter phonon relaxation time. Meanwhile, the incorporation of $AgSbTe_2$ causes a phonon softening effect, and the phonon group velocity decreases upon $AgSbTe_2$ alloying (Table S2).

The transmission electron microscopy (TEM) analysis was carried out on the optimal $y = 15$ sample to reveal the atomic-scale microstructure. As presented in Fig. 5a, distinct domain regions with varying bright and dark contrasts are observed, which is a typical feature of GeTe alloys. [65] Furthermore, obvious dislocations (marked by red arrows) can be observed in this sample (Fig. 5b). To further investigate the microstructure in atomic scale, the high-angle annular dark-field (HAADF) STEM image are presented in Fig. 5c and Fig. 5 f. A distinctly different atomic arrangement was found in

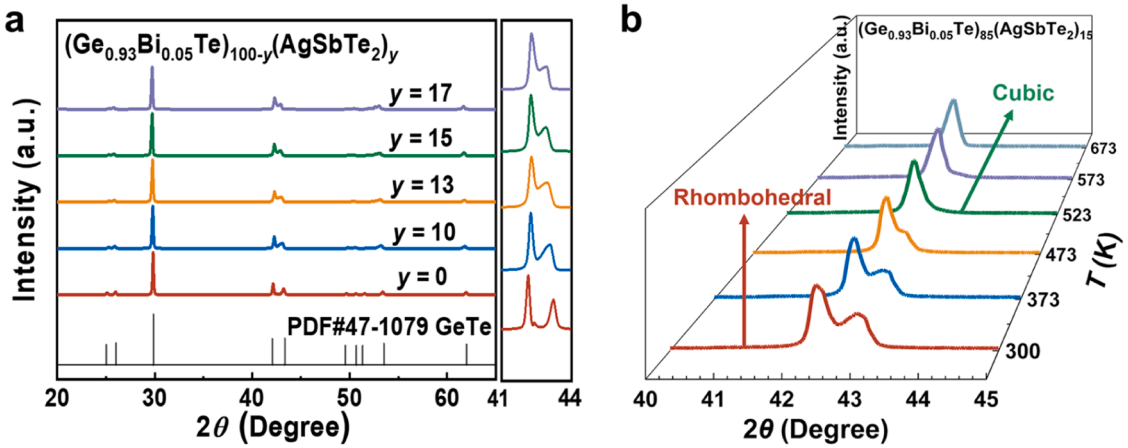

Fig. 3. Evolution of the crystal structure upon $AgSbTe_2$ alloying. **a,** Room-temperature XRD patterns of $(Ge_{0.93}Bi_{0.05}Te)_{100-y}(AgSbTe_2)_y$ ($y = 0$, 10, 13, 15, and 17) and the enlarged view of the 2θ peaks in the range of 41–44°. **b,** Temperature-dependent XRD patterns for $(Ge_{0.93}Bi_{0.05}Te)_{85}(AgSbTe_2)_{15}$.

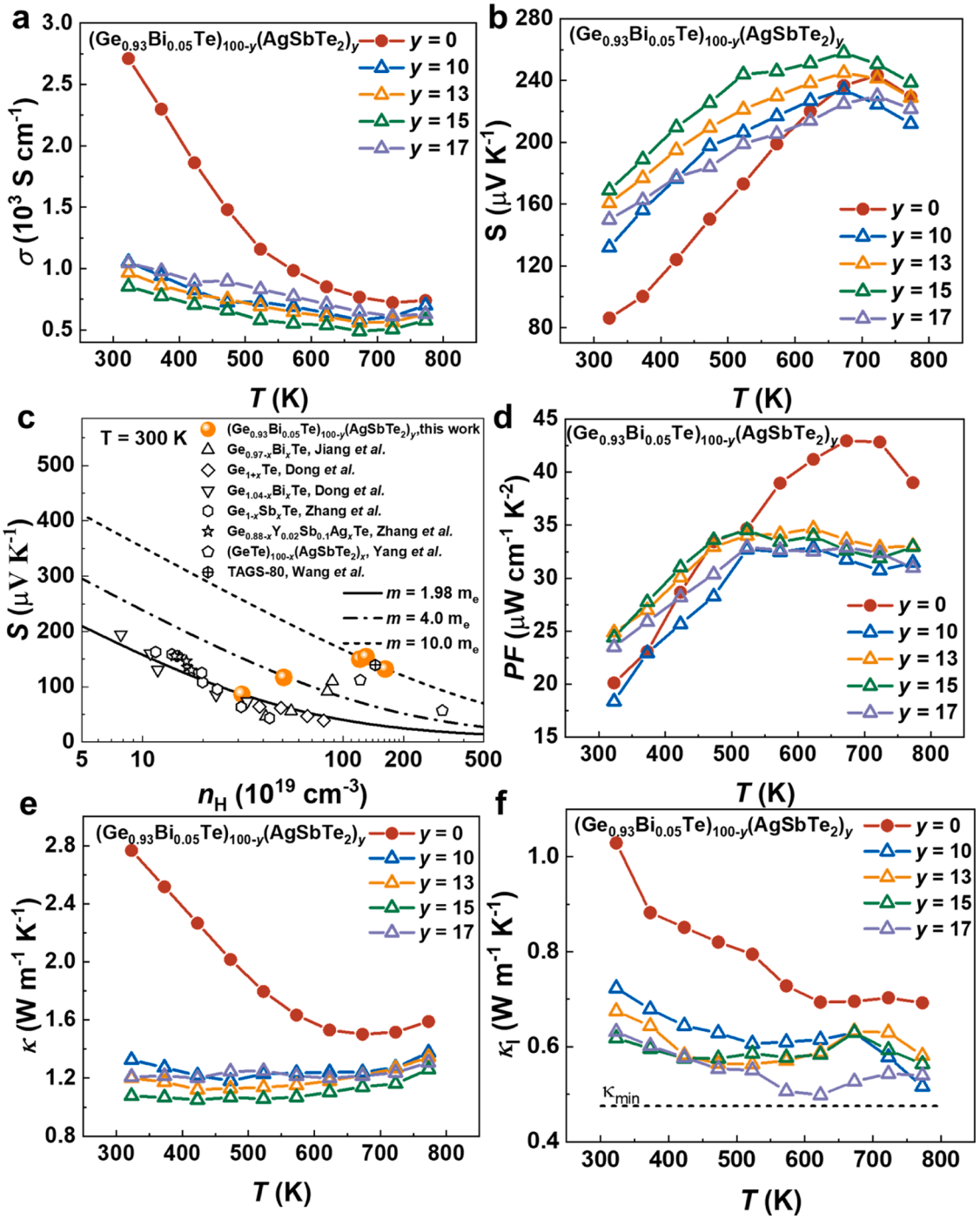

Fig. 4. Temperature-dependent thermoelectric performance and Pisarenko relations for the $AgSbTe_2$-alloyed $Ge_{0.93}Bi_{0.05}Te$. **a**, Electrical conductivity. **b**, Seebeck coefficient. **d**, Power factor. **e**, Total thermal conductivity. **f**, Lattice thermal conductivity. **c**, The Hall carrier concentration-dependent Seebeck coefficient of $(Ge_{0.93}Bi_{0.05}Te)_{100-y}(AgSbTe_2)_y$ ($y = 0$, 10, 13, 15, and 17) compared to the reported values of other GeTe-based materials with similar chemical compositions. [18, 52,59–61,63].

$(Ge_{0.93}Bi_{0.05}Te)_{85}(AgSbTe_2)_{15}$, as indicated by the yellow square in Fig. 5c. To further know the constituents of this region, the fast Fourier transform (FFT) patterns of Fig. 5c and the region in yellow square are shown in Figs. 5d and 5e, respectively. Through the comparison between the standard electron diffraction patterns and the experimental FFT images, it is indicated that the region in yellow square is cubic GeTe (C-GeTe). Additionally, the measurement of the angle between specific diffraction spots in FFT images corresponds well with the standard electron diffraction patterns (92.3° for R-GeTe along the [100] zone axis, and 90° for C-GeTe along the [110] zone axis), confirming the co-existence of C-GeTe and R-GeTe in this sample. Moreover, the geometric phase analysis (GPA) mapping of Fig. 5c along the *xx* (Fig. 5 g), reveals that high alloying concentration and the phase interface between R-GeTe and C-GeTe induce large strain fluctuations, leading to strengthened phonon scattering. The phonon transport can be significantly impeded through multiscale hierarchical structures including atomic-scale lattice mismatch, submicron-scale domain structures, and microscale dislocations, resulting in a large reduction in the lattice thermal conductivity.

To further assess the function of $AgSbTe_2$ alloying in manipulating

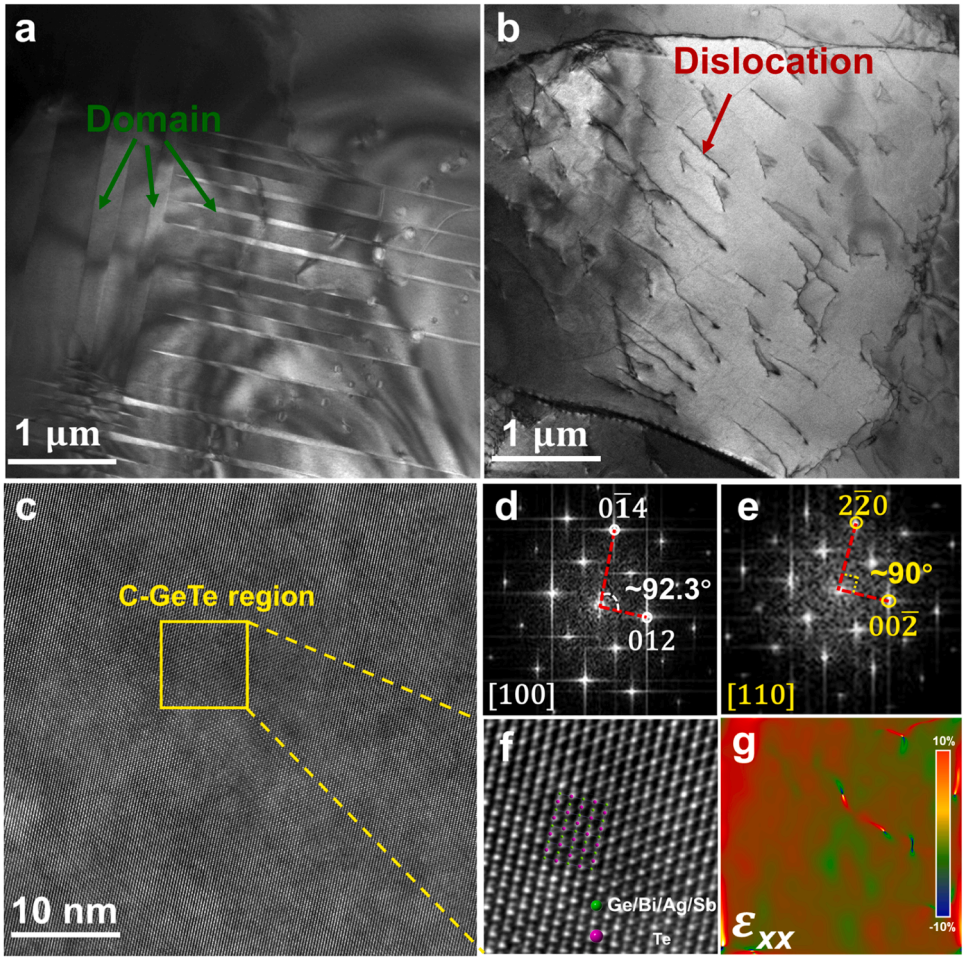

Fig. 5. Microstructures and strain distribution in $(Ge_{0.93}Bi_{0.05}Te)_{85}(AgSbTe_2)_{15}$. **a**, **b**, Low-magnification TEM images. **c**, High-magnification HAADF-STEM image. **d**, **e**, Fast Fourier transformed (FFT) patterns of **c** and the region in yellow square in **c**, respectively. **f**, Magnified image of the yellow square region in c. **g**, Strain mapping of **c** along *xx* direction.

electrical and thermal transport performance, the quality factor (B) of $AgSbTe_2$-alloyed samples is calculated using the following relationship: [66]

$$B = \left(\frac{k_B}{e}\right)^2 \frac{8\pi e(2m_e k_B T)^{3/2}}{3h^3} \frac{\mu_w}{\kappa_l} T \quad (1)$$

where k_B, h, m_e, e, μ_w, κ_l, and T denote the Boltzmann constant, Planck constant, electron mass, electronic charge, the weighted mobility, lattice thermal conductivity, and absolute temperature, respectively. As displayed in Fig. 6a, a significant enhancement of B is observed within the whole low-temperature range after alloying with $AgSbTe_2$. When $y = 15$, B obtains the maximum value among all samples at different temperatures. As a result, with synergistic optimization of electrical and thermal performance, a high zT of 0.73 at 323 K and a zT_{avg} of 1.34 are achieved in $(Ge_{0.93}Bi_{0.05}Te)_{85}(AgSbTe_2)_{15}$ within the low-temperature range (323–573 K) among lead-free GeTe-based materials, as demonstrated in Fig. 6b. To confirm the superiority of the GeTe-based material, a single-leg device was fabricated to estimate energy conversion performance. As illustrated in Fig. 6c, the *I-U* curve exhibits good linearity, allowing for accurate determination of the open-circuit voltage (U_{oc}, by the intercept) and internal resistance (R_{in}, by the slope) of the single-leg device. Furthermore, a maximum power (P) of 0.09 W accompanied by a power density (P_d) of 0.62 W cm^{-2} and a maximum η (η_{max}) of 8.6 % under a ΔT of 273 K are achieved (Fig. 6c, d).

3. Conclusion

In summary, synergistic optimization between electrical and thermal transport is realized in GeTe. On the basis of Bi doping, the introduction of Ge deficiency effectively modulates the band structure and strengthens the phonon scattering, resulting in a peak zT of 2.04 at 723 K. Further $AgSbTe_2$ alloying facilitates the phase transition, and significantly increases the density-of-states effective mass m^*, resulting in an outstanding μ_w of 183 $cm^2V^{-1}s^{-1}$ at 323 K. High alloying concentration introduces complex hierarchical structures, strongly blocking phonon transport, contributing to a substantial reduction in the lattice thermal conductivity. Consequently, a zT of 0.73 at 323 K and a high zT_{avg} of 1.34 (323–573 K) are achieved in $(Ge_{0.93}Bi_{0.05}Te)_{85}(AgSbTe_2)_{15}$. The single leg exhibits an outstanding energy conversion efficiency of 8.6 % among the lead-free GeTe-based materials. This study offers an opportunity for GeTe-based materials to emerge as a rival to the commercial Bi_2Te_3-based alloys in low-grade waste heat recovery applications.

CRediT authorship contribution statement

Haiqi Li: Writing – review & editing, Writing – original draft, Visualization, Software, Methodology, Formal analysis, Data curation. **Chen Chen**: Writing – review & editing, Visualization, Supervision, Software, Resources, Investigation, Formal analysis. **Jinxuan Cheng**: Writing – review & editing, Software, Formal analysis, Data curation.

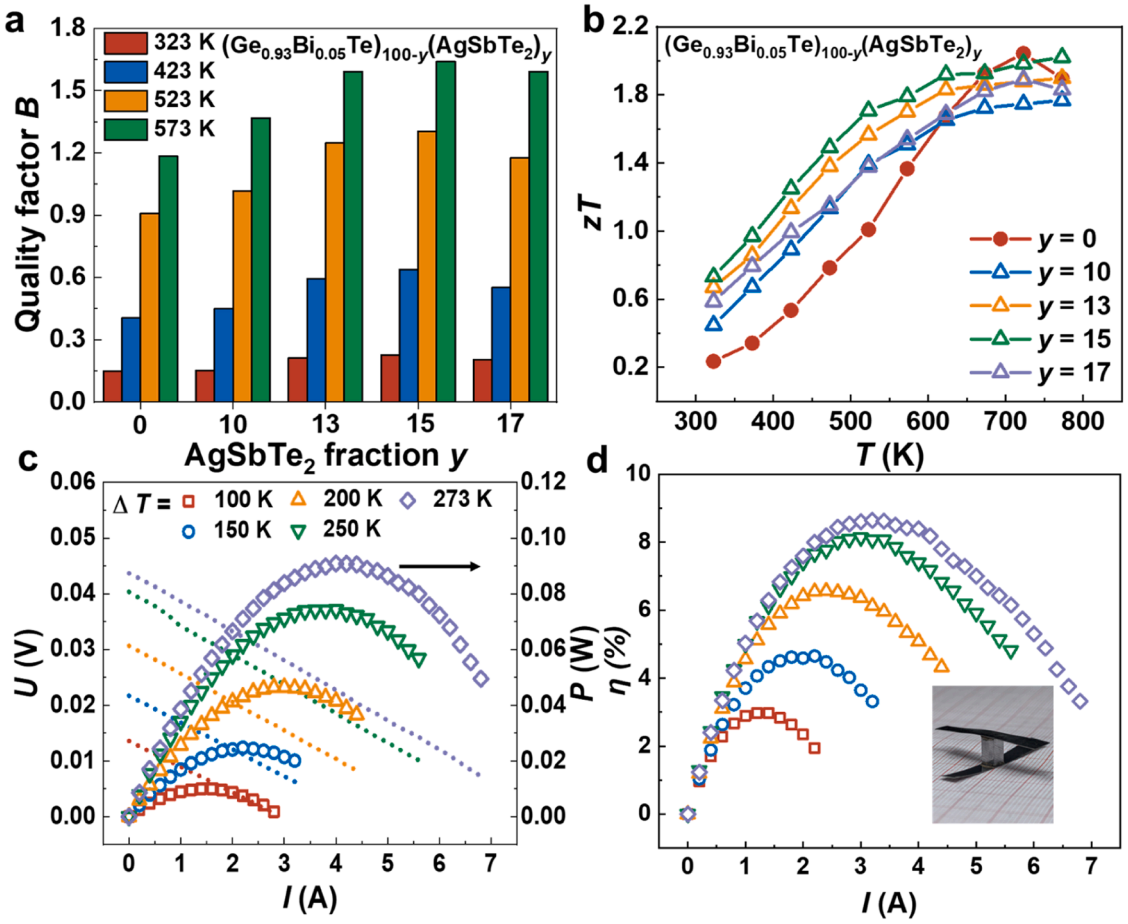

Fig. 6. Thermoelectric performance and device properties of the single leg. **a**, Quality factor. **b**, Temperature-dependent zT values of $(Ge_{0.93}Bi_{0.05}Te)_{100-y}(AgSbTe_2)_y$ ($y = 0$, 10, 13, 15, and 17) samples. Measured current-dependent **c** output voltage and power, and **d** conversion efficiency, collected on a single leg using the sample $(Ge_{0.93}Bi_{0.05}Te)_{85}(AgSbTe_2)_{15}$ at various temperature differences (ΔT).

Yuanhang Xia: Writing – review & editing, Software, Investigation. **Shuang Lyu**: Software, Methodology, Investigation, Formal analysis. **Kejia Liu**: Software, Resources. **Wenhua Xue**: Software, Resources, Investigation. **Dongyi Shen**: Visualization, Resources. Wenxuan Wang: Visualization, Validation. **Qian Zhang**: Writing – review & editing, Supervision, Resources, Project administration. **Yue Chen**: Writing – review & editing, Visualization, Supervision, Resources, Project administration, Investigation, Formal analysis, Data curation.

Declaration of Competing Interest

The authors declare that they have no known competing financial interests or personal relationships that could have appeared to influence the work reported in this paper.

Acknowledgements

This work is supported by the Research Grants Council of Hong Kong (C7002–22Y, 17318122, and C6020–22GF).

Appendix A. Supporting information

Supplementary data associated with this article can be found in the online version at doi:10.1016/j.nanoen.2025.110690.

Data availability

Data will be made available on request.

References

[1] G. Schierning, Bring on the heat, Nat. Energy 3 (2) (2018) 92–93.
[2] W.-D. Liu, L.-C. Yin, L. Li, Q. Yang, D.-Z. Wang, M. Li, X.-L. Shi, Q. Liu, Y. Bai, I. Gentle, Grain boundary re-crystallization and sub-nano regions leading to high plateau figure of merit for Bi_2Te_3 nanoflakes, Energy Environ. Sci. 16 (11) (2023) 5123–5135.
[3] X. Wu, Y. Lin, C. Liu, Y. Wang, H. Li, B. Ge, W. Liu, High performance eco-friendly MgAgSb-based thermoelectric power generation device near phase transition temperatures, Energy Environ. Sci. (2024).
[4] X. Li, C. Chen, L. Yin, X. Wang, J. Mao, F. Cao, Q. Zhang, Realizing an excellent conversion efficiency of 14.5% in the Mg 3 Sb 2/GeTe-based thermoelectric module for waste heat recovery, Energy Environ. Sci. 16 (12) (2023) 6147–6154.
[5] S. Liu, Y. Wen, S. Bai, H. Shi, Y. Qin, B. Qin, D. Liu, Q. Cao, X. Gao, L. Su, C. Chang, X. Zhang, L.D. Zhao, Lattice plainification leads to high thermoelectric performance of P-type PbSe crystals, Adv. Mater. (2024) e2401828.
[6] S. Roychowdhury, T. Ghosh, R. Arora, M. Samanta, L. Xie, N.K. Singh, A. Soni, J. He, U.V. Waghmare, K. Biswas, Enhanced atomic ordering leads to high thermoelectric performance in AgSbTe2, Science 371 (6530) (2021) 722–727.
[7] D. Liu, D. Wang, T. Hong, Z. Wang, Y. Wang, Y. Qin, L. Su, T. Yang, X. Gao, Z. Ge, Lattice plainification advances highly effective SnSe crystalline thermoelectrics, Science 380 (6647) (2023) 841–846.
[8] L.C. Yin, W.D. Liu, M. Li, D.Z. Wang, S. Li, S.Q. Li, X.L. Shi, Y. Wang, L. Zhang, Q. Liu, Bipolar suppression for high performance n-type GeTe-based thermoelectrics, *Adv. Energy Mater.* (2024) 2400340.
[9] U.S. Shenoy, D.K. Bhat, Tuning the electronic structure of rhombohedral and cubic GeTe for thermoelectric application: influence of molybdenum doping, J. Phys. Chem. Solids 188 (2024) 111943.
[10] D.K. Bhat, U.S. Shenoy, Mg/Ca doping ameliorates the thermoelectric properties of GeTe: influence of electronic structure engineering, J. Alloy. Compd. 843 (2020) 155989.
[11] W.D. Liu, D.Z. Wang, Q. Liu, W. Zhou, Z. Shao, Z.G. Chen, High-performance GeTe-based thermoelectrics: from materials to devices, Adv. Energy Mater. 10 (19) (2020) 2000367.
[12] D.K. Bhat, U.S. Shenoy, Resonance levels in GeTe thermoelectrics: zinc as a new multifaceted dopant, N. J. Chem. 44 (41) (2020) 17664–17670.

[13] U.S. Shenoy, D.K. Bhat, Probing of Bi doped GeTe thermoelectrics leads to revelation of resonant states, J. Alloy. Compd. 921 (2022) 165965.
[14] L.C. Yin, W.D. Liu, M. Li, D.Z. Wang, H. Wu, Y. Wang, L. Zhang, X.L. Shi, Q. Liu, Z. G. Chen, Interstitial Cu: an effective strategy for high carrier mobility and high thermoelectric performance in GeTe, Adv. Funct. Mater. 33 (25) (2023) 2301750.
[15] D.Z. Wang, W.D. Liu, M. Li, K. Zheng, H. Hu, L.C. Yin, Y. Wang, H. Zhu, X.L. Shi, X. Yang, Hierarchical architectural structures induce high performance in n-type GeTe-based thermoelectrics, Adv. Funct. Mater. 33 (14) (2023) 2213040.
[16] D.-Z. Wang, W.-D. Liu, Y. Mao, S. Li, L.-C. Yin, H. Wu, M. Li, Y. Wang, X.-L. Shi, X. Yang, Decoupling carrier-phonon scattering boosts the thermoelectric performance of n-type GeTe-based materials, J. Am. Chem. Soc. 146 (2) (2024) 1681–1689.
[17] L. Xie, Y. Chen, R. Liu, E. Song, T. Xing, T. Deng, Q. Song, J. Liu, R. Zheng, X. Gao, Stacking faults modulation for scattering optimization in GeTe-based thermoelectric materials, Nano Energy 68 (2020) 104347.
[18] Y. Jiang, J. Dong, H.L. Zhuang, J. Yu, B. Su, H. Li, J. Pei, F.H. Sun, M. Zhou, H. Hu, J.W. Li, Z. Han, B.P. Zhang, T. Mori, J.F. Li, Evolution of defect structures leading to high ZT in GeTe-based thermoelectric materials, Nat. Commun. 13 (1) (2022) 6087.
[19] C. Zhu, J. Wang, F. Luo, S. Zhang, J. Wang, Y. Zhang, H. Liu, Z. Sun, Enhanced thermoelectric performance of GeTe-based composites incorporated with Fe nanoparticles, ACS Appl. Mater. Interfaces 14 (34) (2022) 38854–38864.
[20] Z. Bu, Z. Chen, X. Zhang, S. Lin, J. Mao, W. Li, Y. Chen, Y. Pei, Near-room-temperature rhombohedral Ge1-xPbxTe thermoelectrics, Mater. Today Phys. 15 (2020) 100260.
[21] B. Jiang, W. Wang, S. Liu, Y. Wang, C. Wang, Y. Chen, L. Xie, M. Huang, J. He, High figure-of-merit and power generation in high-entropy GeTe-based thermoelectrics, Science 377 (6602) (2022) 208–213.
[22] Y. Qiu, Y. Jin, D. Wang, M. Guan, W. He, S. Peng, R. Liu, X. Gao, L.-D. Zhao, Realizing high thermoelectric performance in GeTe through decreasing the phase transition temperature via entropy engineering, J. Mater. Chem. A 7 (46) (2019) 26393–26401.
[23] M. Liu, J. Zhu, B. Cui, F. Guo, Z. Liu, Y. Zhu, M. Guo, Y. Sun, Q. Zhang, Y. Zhang, High-performance lead-free cubic GeTe-based thermoelectric alloy, Cell Rep. Phys. Sci. 3 (6) (2022).
[24] S. Duan, W. Xue, H. Yao, X. Wang, C. Wang, S. Li, Z. Zhang, L. Yin, X. Bao, L. Huang, Achieving high thermoelectric performance by $NaSbTe_2$ alloying in GeTe for simultaneous suppression of Ge vacancies and band tailoring, Adv. Energy Mater. 12 (3) (2022) 2103385.
[25] N. Li, W. He, C. Li, G. Wang, G. Wang, X. Zhou, X. Lu, The role of electronegativity in the thermoelectric performance of GeTe–I–V–VI_2 solid solutions, J. Mater. Chem. A 9 (4) (2021) 2385–2393.
[26] C. Zhang, G. Yan, Y. Wang, X. Wu, L. Hu, F. Liu, W. Ao, O. Cojocaru-Mirédin, M. Wuttig, G.J. Snyder, Grain boundary complexions enable a simultaneous optimization of electron and phonon transport leading to high-performance GeTe thermoelectric devices, Adv. Energy Mater. 13 (3) (2023) 2203361.
[27] Z. Guo, G. Wu, X. Tan, R. Wang, Z. Zhang, G. Wu, Q. Zhang, J. Wu, G.Q. Liu, J. Jiang, Enhanced thermoelectric performance in GeTe by synergy of midgap state and band convergence, Adv. Funct. Mater. 33 (11) (2023) 2212421.
[28] Y. Jin, D. Wang, T. Hong, L. Su, H. Shi, S. Zhan, Y. Wang, S. Wang, X. Gao, Y. Qiu, Outstanding CdSe with multiple functions leads to high performance of GeTe thermoelectrics, Adv. Energy Mater. 12 (10) (2022) 2103779.
[29] Y. Jin, T. Hong, D. Wang, Y. Xiao, W. He, X. Gao, Y. Qiu, L.-D. Zhao, Band structure and microstructure modulations enable high quality factor to elevate thermoelectric performance in $Ge_{0.9}Sb_{0.1}Te$-x% $FeTe_2$, Mater. Today Phys. 20 (2021) 100444.
[30] L. Wu, X. Li, S. Wang, T. Zhang, J. Yang, W. Zhang, L. Chen, J. Yang, Resonant level-induced high thermoelectric response in indium-doped GeTe, Npg Asia Mater. 9 (1) (2017) e343. -e343.
[31] D. Wu, L.-D. Zhao, S. Hao, Q. Jiang, F. Zheng, J.W. Doak, H. Wu, H. Chi, Y. Gelbstein, C. Uher, Origin of the high performance in GeTe-based thermoelectric materials upon Bi_2Te_3 doping, J. Am. Chem. Soc. 136 (32) (2014) 11412–11419.
[32] Z. Zheng, X. Su, R. Deng, C. Stoumpos, H. Xie, W. Liu, Y. Yan, S. Hao, C. Uher, C. Wolverton, Rhombohedral to cubic conversion of GeTe via MnTe alloying leads to ultralow thermal conductivity, electronic band convergence, and high thermoelectric performance, J. Am. Chem. Soc. 140 (7) (2018) 2673–2686.
[33] T. Zhang, N. Qi, X. Su, X. Tang, Z. Chen, Vacancy suppression induced synergetic optimization of thermoelectric performance in Sb-doped GeTe evidenced by positron annihilation spectroscopy, ACS Appl. Mater. Interfaces 15 (34) (2023) 40665–40675.
[34] C. Liu, Z. Zhang, Y. Peng, F. Li, L. Miao, E. Nishibori, R. Chetty, X. Bai, R. Si, J. Gao, Charge transfer engineering to achieve extraordinary power generation in GeTe-based thermoelectric materials, Sci. Adv. 9 (17) (2023) eadh0713.
[35] Z. Liu, J. Sun, J. Mao, H. Zhu, W. Ren, J. Zhou, Z. Wang, D.J. Singh, J. Sui, C.-W. Chu, Phase-transition temperature suppression to achieve cubic GeTe and high thermoelectric performance by Bi and Mn codoping, Proc. Natl. Acad. Sci. 115 (21) (2018) 5332–5337.
[36] M. Hong, Z.G. Chen, L. Yang, Y.C. Zou, M.S. Dargusch, H. Wang, J. Zou, Realizing zT of 2.3 in $Ge_{1-x-y}Sb_xIn_yTe$ via reducing the phase-transition temperature and introducing resonant energy doping, Adv. Mater. 30 (11) (2018) 1705942.
[37] Y. Jiang, J. Dong, H.-L. Zhuang, J. Yu, B. Su, H. Li, J. Pei, F.-H. Sun, M. Zhou, H. Hu, Evolution of defect structures leading to high ZT in GeTe-based thermoelectric materials, Nat. Commun. 13 (1) (2022) 6087.
[38] X. Xu, L. Xie, Q. Lou, D. Wu, J. He, Boosting the thermoelectric performance of pseudolayered Sb_2Te_3 $(GeTe)_n$ via vacancy engineering, Adv. Sci. 5 (12) (2018) 1801514.
[39] B. Zhu, W. Wang, J. Cui, J. He, Point defect engineering: Co-doping synergy realizing superior performance in n-Type Bi_2Te_3 thermoelectric materials, Small 17 (29) (2021) 2101328.
[40] X. Lu, Q. Zhang, J. Liao, H. Chen, Y. Fan, J. Xing, S. Gu, J. Huang, J. Ma, J. Wang, High-efficiency thermoelectric power generation enabled by homogeneous incorporation of MXene in (Bi, Sb)$_2$Te$_3$ matrix, Adv. Energy Mater. 10 (2) (2020) 1902986.
[41] F. Hao, P. Qiu, Y. Tang, S. Bai, T. Xing, H.-S. Chu, Q. Zhang, P. Lu, T. Zhang, D. Ren, High efficiency Bi_2Te_3-based materials and devices for thermoelectric power generation between 100 and 300°C, *Energy Environ. Sci.* 9 (10) (2016) 3120–3127.
[42] R. Deng, X. Su, S. Hao, Z. Zheng, M. Zhang, H. Xie, W. Liu, Y. Yan, C. Wolverton, C. Uher, High thermoelectric performance in $Bi_{0.46}Sb_{1.54}Te_3$ nanostructured with ZnTe, Energy Environ. Sci. 11 (6) (2018) 1520–1535.
[43] T. Kuroki, K. Kabeya, K. Makino, T. Kajihara, H. Kaibe, H. Hachiuma, H. Matsuno, A. Fujibayashi, Thermoelectric generation using waste heat in steel works, J. Electron. Mater. 43 (2014) 2405–2410.
[44] Y.K. Zhu, Y. Sun, J. Zhu, K. Song, Z. Liu, M. Liu, M. Guo, X. Dong, F. Guo, X. Tan, Mediating point defects endows n-Type Bi_2Te_3 with high thermoelectric performance and superior mechanical robustness for power generation application, Small 18 (23) (2022) 2201352.
[45] B. Zhu, X. Liu, Q. Wang, Y. Qiu, Z. Shu, Z. Guo, Y. Tong, J. Cui, M. Gu, J. He, Realizing record high performance in n-type Bi_2Te_3-based thermoelectric materials, Energy Environ. Sci. 13 (7) (2020) 2106–2114.
[46] A.K. Bohra, R. Bhatt, A. Singh, S. Bhattacharya, R. Basu, K. Meshram, S.K. Sarkar, P. Bhatt, P. Patro, D. Aswal, Transition from n-to p-type conduction concomitant with enhancement of figure-of-merit in Pb doped bismuth telluride: Material to device development, Mater. Des. 159 (2018) 127–137.
[47] G. Bulman, B. Cook, High-efficiency energy harvesting using TAGS-85/half-Heusler thermoelectric devices. Energy Harvesting and Storage: Materials, Devices, and Applications V, SPIE, 2014, pp. 17–24.
[48] T. Xing, Q. Song, P. Qiu, Q. Zhang, M. Gu, X. Xia, J. Liao, X. Shi, L. Chen, High efficiency GeTe-based materials and modules for thermoelectric power generation, Energy Environ. Sci. 14 (2) (2021) 995–1003.
[49] C. Li, S. Ma, P. Wei, W. Zhu, X. Nie, X. Sang, Z. Sun, Q. Zhang, W. Zhao, Magnetism-induced huge enhancement of the room-temperature thermoelectric and cooling performance of p-type BiSbTe alloys, Energy Environ. Sci. 13 (2) (2020) 535–544.
[50] Z. Guo, K. Song, Z. Yan, P. Sun, X. Tan, G. Wu, Q. Zhang, G.-Q. Liu, B. Yu, J. Jiang, Broadening the optimum thermoelectric power generation range of p-type sintered $Bi_{0.4}Sb_{1.6}Te_3$ by suppressing bipolar effect, Chem. Eng. J. 426 (2021) 131853.
[51] J.R. Salvador, J. Yang, X. Shi, H. Wang, A. Wereszczak, Transport and mechanical property evaluation of (AgSbTe) 1− x (GeTe) x (x= 0.80, 0.82, 0.85, 0.87, 0.90), J. Solid State Chem. 182 (8) (2009) 2088–2095.
[52] X.Y. Wang, H.H. Yao, L. Yin, W.H. Xue, Z.W. Zhang, S.C. Duan, L.J. Chen, C. Chen, J.H. Sui, X.J. Liu, Y.M. Wang, J. Mao, Q. Zhang, X. Lin, Band modulation and strain fluctuation for realizing high average in GeTe, Adv. Energy Mater. 12 (26) (2022).
[53] H. Kim, S.K. Kihoi, U.S. Shenoy, J.N. Kahiu, D.H. Shin, D.K. Bhat, H.S. Lee, High thermoelectric and mechanical performance achieved by a hyperconverged electronic structure and low lattice thermal conductivity in GeTe through CuInTe 2 alloying, J. Mater. Chem. A 11 (15) (2023) 8119–8130.
[54] G.A. Slack, D. Rowe, CRC handbook of thermoelectrics, CRC press, Boca Raton, FL, 1995.
[55] T. Zhang, S. Deng, X. Zhao, X. Ruan, N. Qi, Z. Chen, X. Su, X. Tang, Regulation of Ge vacancies through Sm doping resulting in superior thermoelectric performance in GeTe, J. Mater. Chem. A 10 (7) (2022) 3698–3709.
[56] Y.-F. Tsai, Y.-C. Chao, C.-R. Hsing, K.-K. Wang, Y.-H. Tung, C.-C. Yang, S.-W. Chen, G.J. Snyder, H.-W. Yen, C.-M. Wei, P.-C. Wei, H.-J. Wu, From stoichiometric to off-stoichiometric GeTe: phase diagram reconstruction and thermoelectric performance reassessment, Acta Mater. 265 (2024).
[57] J. Li, X. Zhang, Z. Chen, S. Lin, W. Li, J. Shen, I.T. Witting, A. Faghaninia, Y. Chen, A. Jain, Low-symmetry rhombohedral GeTe thermoelectrics, Joule 2 (5) (2018) 976–987.
[58] B.A. Cook, X. Wei, J.L. Harringa, M.J. Kramer, In-situ elevated-temperature TEM study of $(AgSbTe_2)_{15}(GeTe)_{85}$, J. Mater. Sci. 42 (2007) 7643–7646.
[59] C. Liu, Z. Zhang, Y. Peng, F. Li, L. Miao, E. Nishibori, R. Chetty, X. Bai, R. Si, J. Gao, X. Wang, Y. Zhu, N. Wang, H. Wei, T. Mori, Charge transfer engineering to achieve extraordinary power generation in GeTe-based thermoelectric materials, Sci. Adv. 9 (17) (2023) eadh0713.
[60] T. Zhang, N. Qi, X. Su, X. Tang, Z. Chen, Vacancy suppression induced synergetic optimization of thermoelectric performance in Sb-doped GeTe evidenced by positron annihilation spectroscopy, ACS Appl. Mater. Interfaces 15 (34) (2023) 40665–40675.
[61] J.F. Dong, F.H. Sun, H.C. Tang, J. Pei, H.L. Zhuang, H.H. Hu, B.P. Zhang, Y. Pan, J. F. Li, Medium-temperature thermoelectric GeTe: vacancy suppression and band structure engineering leading to high performance, Energy Environ. Sci. 12 (4) (2019) 1396–1403.
[62] G. Tan, L.-D. Zhao, M.G. Kanatzidis, Rationally designing high-performance bulk thermoelectric materials, Chem. Rev. 116 (19) (2016) 12123–12149.
[63] S.H. Yang, T. Zhu, T. Sun, J. He, S. Zhang, X. Zhao, Nanostructures in high-performance (GeTe) x (AgSbTe2) 100− x thermoelectric materials, Nanotechnology 19 (24) (2008) 245707.

[64] D.G. Cahill, S.K. Watson, R.O. Pohl, Lower limit to the thermal conductivity of disordered crystals, Phys. Rev. B 46 (10) (1992) 6131.
[65] H.S. Lee, B.-S. Kim, C.-W. Cho, M.-W. Oh, B.-K. Min, S.-D. Park, H.-W. Lee, Herringbone structure in GeTe-based thermoelectric materials, Acta Mater. 91 (2015) 83–90.
[66] Y. Pei, H. Wang, G.J. Snyder, Band engineering of thermoelectric materials, Adv. Mater. 24 (46) (2012) 6125–6135.